

Spatial interference between pairs of optical paths with a chaotic source

Michele Cassano

Dipartimento Interateneo di Fisica, Università degli Studi di Bari, 70100 Bari, Italy

E-mail: m.cassano28@studenti.uniba.it

Milena D'Angelo

Dipartimento Interateneo di Fisica, Università degli Studi di Bari, 70100 Bari, Italy

Istituto Nazionale Di Fisica Nucleare, sez. di Bari, 70100 Bari, Italy

Augusto Garuccio

Dipartimento Interateneo di Fisica, Università degli Studi di Bari, 70100 Bari, Italy

Istituto Nazionale Di Fisica Nucleare, sez. di Bari, 70100 Bari, Italy

Tao Peng

Department of Physics, University of Maryland, Baltimore County, Baltimore, MD
21250, USA

Yanhua Shih

Department of Physics, University of Maryland, Baltimore County, Baltimore, MD
21250, USA

Vincenzo Tamma

Institut für Quantenphysik and Center for Integrated Quantum Science and
Technology (IQST), Universität Ulm, D-89069 Ulm, Germany

E-mail: vincenzo.tamma@uni-ulm.de

Abstract. We demonstrate a second-order spatial interference effect with a chaotic source. This phenomenon arises from the indistinguishability between pairs of optical paths emerging from correlation measurements in the photon-number fluctuations. We show how this effect can be used to simulate a controlled-*NOT* gate, as well as arbitrary-order on-demand entanglement correlations in more complex interferometric networks.

1. Introduction

The fundamental physics of temporal and spatial coherence and interference with thermal light is at the very heart of the experiments performed in the mid-1950s by Hanbury Brown and Twiss. These experiments trigger the development of the quantum optics field [1, 2, 3, 4]. Indeed, in the last 60 years, numerous fundamental studies [5, 6, 7, 8, 9, 10] of the physics of multi-photon interference have been performed, with applications in imaging [11, 12, 13, 14, 15], quantum information processing [16, 17, 18, 19, 20], metrology [21, 22], N-photon tomography, entanglement generation [9, 23] and entanglement simulation [24, 25, 26, 27, 28].

Recently, a second-order correlation phenomenon based on the interference between pairs of optical paths has been demonstrated [10] in the temporal domain with a chaotic source, providing a deeper fundamental understanding of the physics of second-order coherence beyond the Hanbury Brown and Twiss effect. As shown in [10], this phenomena can be also used to simulate a controlled-NOT (CNOT) gate operation [29, 30, 31].

In this paper, we demonstrate theoretically a second-order interference effect in the spatial domain analogous to the one demonstrated in the temporal domain [10]. The propose interferometer (see Fig.1) is characterized by two identical two-pinhole masks illuminated by chaotic light, and placed in two separate arms. We show that second order interference between two pairs of indistinguishable optical paths can be observed by performing correlation measurements at the interferometer output (sect.2). The distance between the two pinholes in both masks is larger than the transverse coherence length of the chaotic source. Hence, no first order interference exists behind each mask. Furthermore we demonstrate that the proposed interference phenomenon can be used (Fig. 2) to simulate a particular class of controlled-unitary gates and, particularly, a CNOT gate. In (sect. 3), we also propose a modified setup (Fig. 3) that can be used for the simulation of higher-order interferometric networks.

2. Basic interference effect

In the proposed interferometer (Fig.1), chaotic light is split by a balanced non-polarizing beam-splitter. Two identical two-pinhole masks are placed, in the output arms of the beam-splitter, at the same distance z from the source, in its near field. The pinholes at the positions are indicated as 1,2 for the upper mask and 1',2' for the lower mask. The light transmitted by the masks reaches two point-like detectors, D_C and D_T , placed at the same distance f from the masks. A correlation measurement in the fluctuation of the number of photons is finally performed. Let us start by evaluating the second order correlation function [33, 15]

$$\begin{aligned} G^{(2)}(x_i, x_j) &\propto \langle n(x_i)n(x_j) \rangle \\ &= \langle n(x_i) \rangle \langle n(x_j) \rangle + \langle \Delta n(x_i)\Delta n(x_j) \rangle, \end{aligned} \quad (1)$$

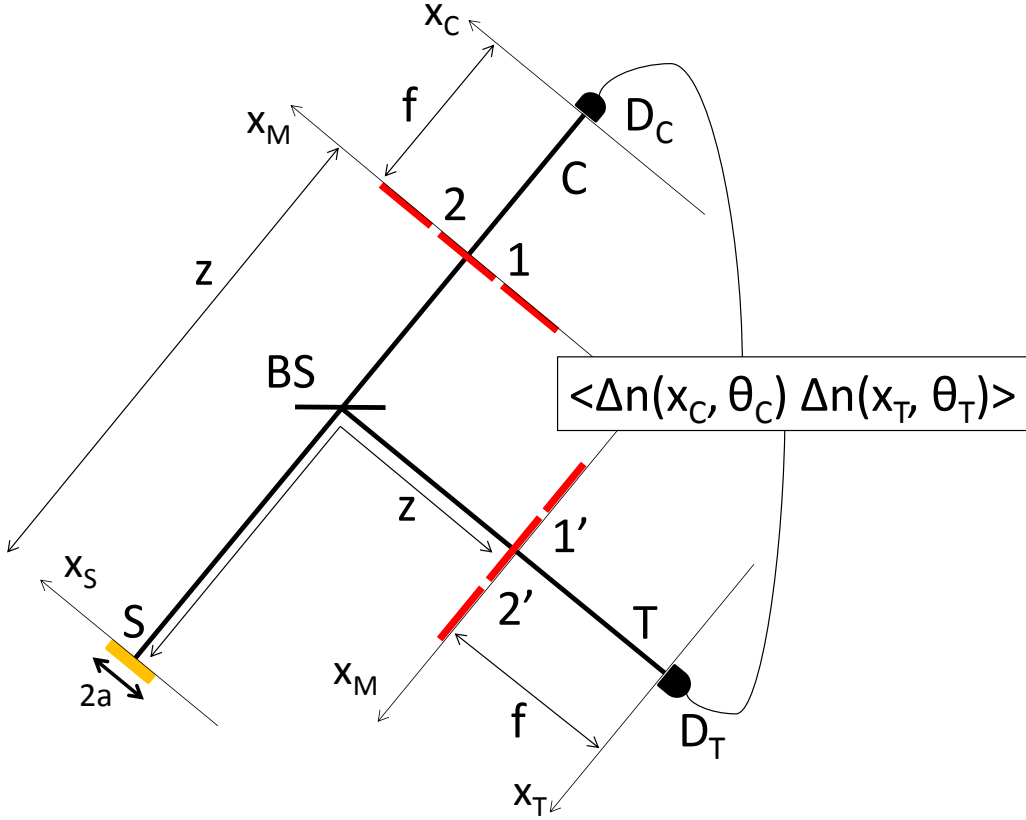


Figure 1. Basic setup for the measurement of spatial second-order interference between pairs of optical paths. The light, produced from a one-dim chaotic source of size $2a$, impinges on a balanced non-polarizing beam splitter and, passing through two identical two-pinhole masks placed at the same distance z from the source, reaches two point-like detectors, placed at distance f from the masks. A correlation measurement in the fluctuation of the number of photons is performed at the detector transverse position x_C and x_T .

with $x_i = x_1, x_2$ and $x_j = x_{1'}, x_{2'}$, where n represents the photon number and Δn the photon number fluctuation around the mean. Since we are only interested in measuring spatial correlations at the interferometer output, the chaotic source S is considered to be monochromatic; moreover, for simplicity, it is assumed to be 1-dim, of length $2a$, and H-polarized. The input chaotic light state is described by [33, 34]

$$\hat{\rho}_H = \int \left[\prod_{\kappa} d^2 \alpha_{\kappa, H} \right] P(\{\alpha_{\kappa, H}\}) \bigotimes_{\kappa} |\alpha_{\kappa, H}\rangle_S \langle \alpha_{\kappa, H}|, \quad (2)$$

with the Glauber-Sudarshan probability distribution [3, 35]

$$P(\{\alpha_{\kappa, H}\}) = \prod_{\kappa} \frac{1}{\pi \langle n_{\kappa} \rangle} \exp \left(-\frac{|\alpha_{\kappa, H}|^2}{\langle n_{\kappa} \rangle} \right), \quad (3)$$

where $\alpha_{\kappa, H}$ are H-polarized coherent states, in the mode κ associated with the x component of the transverse wave vector, and $\langle n_{\kappa} \rangle$ is the corresponding average photon

number. Since the average photon number in a thermal source depends only on the frequency [34], we can assume $\langle n_\kappa \rangle$ to be constant. For quasi-monochromatic chaotic light Eq.(1) reduces to [13]

$$G^{(2)}(x_i, x_j) = G^{(1)}(x_i)G^{(1)}(x_j) + |G^{(1)}(x_i, x_j)|^2, \quad (4)$$

with the $G^{(1)}$ first order correlation function. Therefore $G^{(2)}(x_i, x_j)$ depends on two contributions: the first one, $G^{(1)}(x_i)G^{(1)}(x_j)$, is a constant background; the second one, $|G^{(1)}(x_i, x_j)|^2$, is the interference term. The background can be removed by performing a correlation measurement between the fluctuation of the number of photons [15]. Now an interesting result comes out by working in the hypothesis that

(A) the pinholes, in each mask, are separated by a distance greater than the transverse coherence length of the source (l_{coh}), namely

$$|x_1 - x_{2'}| \gg l_{coh} \quad |x_{1'} - x_2| \gg l_{coh} \quad (5)$$

in such a way that no first order interference can be observed behind each mask;

(B) corresponding pairs of pinholes at the two masks are within the transverse coherence length, which is

$$|x_1 - x_{1'}| \ll l_{coh} \quad |x_2 - x_{2'}| \ll l_{coh}. \quad (6)$$

The outcome of this measurement in the conditions reported in Eq.s (5) and (6) is [14]

$$\langle \Delta I(x_i) \Delta I(x_j) \rangle \neq 0 \Leftrightarrow \begin{cases} (i, j) = (1, 1') \\ (i, j) = (2, 2') \end{cases}, \quad (7)$$

that indicates a maximum correlation for the two pairs of paths (1, 1') and (2, 2') (each one associated with two paths spatially coherent with respect to each other (see Eq. (5))), and no correlation for the configurations (1, 2') and (1', 2).

What happens if we perform correlation measurements after the two-pinholes masks? Intuitively one may expect that the only two possible contributions, associated with the configurations (1, 1') and (2, 2'), would add incoherently. However, if these two contribution are indistinguishable, they sum coherently giving rise to a counter-intuitive interference effect.

To demonstrate this result we evaluate the correlation between the photon the photon-number fluctuations $\Delta n(x_C)$ and $\Delta n(x_T)$, measured at equal detection times, by the detectors D_C and D_T respectively, placed in the transverse position x_C and x_T , behind the two-pinholes masks [33, 15]

$$\begin{aligned} \langle \Delta n(x_C) \Delta n(x_T) \rangle &\propto \langle \Delta I(x_C) \Delta I(x_T) \rangle \\ &= |G^{(1)}(x_C, x_T)|^2, \end{aligned} \quad (8)$$

where

$$G^{(1)}(x_C, x_T) = Tr[\hat{\rho}_H \hat{E}_C^-(x_C) \hat{E}_T^+(x_T)] \quad (9)$$

is the first order correlation function calculated in x_C, x_T , $\hat{E}_d^+(x_d)$ and $\hat{E}_d^-(x_d)$ are, respectively, the positive and negative frequency part of electric field operator at the

position x_d , namely

$$\hat{E}_d^{(+)}(x_d) = \iota \sqrt{\frac{\hbar\omega}{2\epsilon_0}} \int d\kappa e^{-\omega t} \hat{a}_d(\kappa), \quad (10)$$

where ω is the detected frequency, t is the detection time and $\hat{a}_d(\kappa)$ is the annihilation operator associated with the transverse mode κ , at the detector D_d , with $d = C, T$. By propagating the field from the detector to the source plane, we can write

$$\hat{a}_d(\kappa) = g\{\kappa; S, x_d\} \hat{a}_s(\kappa), \quad (11)$$

where $g\{\kappa; S, x_d\}$ is the Green's function that describes the propagation of the mode κ from the source S to the detector D_d , placed in x_d , and $\hat{a}_s(\kappa)$ is the annihilation operator at the source S associated with the mode κ .

As demonstrate in Appendix [Appendix B](#) by using the conditions given in Eq.s (5) and (6), Eq.(8) gives

$$\langle \Delta n(x_C) \Delta n(x_T) \rangle \propto |G_{1,1'}^{(1)}(x_C, x_T) + G_{2,2'}^{(1)}(x_C, x_T)|^2, \quad (12)$$

where $G_{1,1}^{(1)}$ and $G_{2,2'}^{(1)}$ indicate the contributions to the correlation measurement coming from the two pairs of paths(1, 1') and (2, 2') respectively; in fact, we have

$$G_{i,j}^{(1)}(x_C, x_T) \propto B_i^*(x_C) B_j(x_T) \quad (13)$$

$$\times FT \{|A(x_s)|^2\} [(x_i - x_j)/(2al_{coh})], \quad (14)$$

where $B_i^*(x_C)$ and $B_j(x_T)$ are two phase factors (see Eq.(A.9)), $FT \{|A(x_s)|^2\} [\chi]$ represents the Fourier transform, calculated in χ , of the source intensity profile which we have assumed to be constant and different from zero only over an extension $2a$ (see Eq.(B.7)), so that $l_{coh} = \lambda z/(2a)$. Hence, on the one hand, due to the conditions in Eq.s (5), the contributions $G_{1,2'}^{(1)}$ and $G_{1',2}^{(1)}$ are null; on the other hand, the conditions in Eq.(6) guarantee that the contribution $G_{i,i'}^{(1)}$ with $i = 1, 2$, are maximum:

$$\begin{aligned} G_{i,i'}^{(1)} &= 2a B_i^*(x_C) B_{i'}(x_T) \\ G_{1,2'}^{(1)} &= G_{1',2}^{(1)} = 0 \end{aligned} \quad (15)$$

Therefore the correlation between the fluctuation of the number of photons depends on the *interference* between the first order correlation functions associated with the pairs of paths (1, 1') and (2, 2'). In fact, these two pairs of paths are *indistinguishable*, even if they correspond to two different transverse coherence length (or two different coherence areas in the more general 2-dim case). In our setup neither of the two point-like detectors can distinguish light coming from the two pinholes. However, the novelty of the proposed interference effect comes from the indistinguishability between two pairs of paths [(1, 1') and (2, 2')], with the peculiarity that each pair involves the two paths connecting the source with two remote pinholes (1 and 1', or 2 and 2') having a relative distance smaller than the transverse coherence length. Such indistinguishability arises from the fact that each contribution $G_{i,i'}^{(1)}$ (Eq. (13)) depends only on the relative distance $x_i - x_j$, between

the point-like slits i and j as compared to the transverse coherence length. Therefore, in the conditions (5) and (6), only the two pairs of paths $(1, 1')$ and $(2'2')$ have non-zero contribution and interfere (see Eq. (12)).

As show in App.[Appendix B](#), by considering the condition $x_C = x_T = 0$, Eq.(12) reduces to

$$\begin{aligned} \langle \Delta n(0) \Delta n(0) \rangle &\propto \left| e^{i\omega/(2cn)(x_1^2 - x_1'^2)} + e^{i\omega/(2cn)(x_2^2 - x_2'^2)} \right|^2 \\ &= \left| 1 + e^{i\phi(x_1, x_2, x_1', x_2')} \right|^2, \end{aligned} \quad (16)$$

where $1/n = 1/z + 1/f$, and

$$\phi(x_1, x_2, x_1', x_2') = \frac{\omega}{2cn} (x_1^2 + x_2'^2 - x_1'^2 - x_2^2) \quad (17)$$

is a phase factor related with the position of the four pinholes. Interestingly this spatial second order interference effect can be used to retrieve information about the position of each pinhole provided the positions of the other three is known. This would not be possible by measuring the intensity separately at the two interferometer output ports, since no first order interference can be observed. This effect is of interest for imaging and metrology applications.

3. Quantum gate simulation

In this section we demonstrate how the physical effect shown in Eq.(12), at the heart of our work, can be exploited for simulating the operation performed by a controlled- U_ϕ gate, with U_ϕ described by

$$U_\phi := \begin{pmatrix} 0 & e^{i\phi} \\ e^{i\phi} & 0 \end{pmatrix}. \quad (18)$$

Let us describe first a *genuine* controlled- U_ϕ gate. Given two-qubit input state $|\phi_C\rangle_C |\phi_T\rangle_T$, where

$$|\phi_C\rangle_C := \cos \phi_C |H\rangle_C + \sin \phi_C |V\rangle_C,$$

and

$$|\phi_T\rangle_T := \cos \phi_T |H\rangle_T + \sin \phi_T |V\rangle_T,$$

the controlled- U_ϕ gate operates on the input state, giving the following output state [16]

$$\begin{aligned} |\psi\rangle &= \cos \phi_C |H\rangle_C |\phi_T\rangle_T \\ &+ e^{i\phi} \sin \phi_C |V\rangle_C |\phi_T^{(F)}\rangle_T, \end{aligned} \quad (19)$$

where

$$|\phi_T^{(F)}\rangle_T := \sin \phi_T |H\rangle_T + \cos \phi_T |V\rangle_T.$$

The polarization-dependent joint detection probability over the state $|\psi\rangle$ is

$$\begin{aligned} P_{U_\phi} &:= |\langle \theta_C, \theta_T | \psi \rangle|^2 \\ &= |\cos \phi_C \cos \theta_C \cos(\phi_T - \theta_T) \\ &\quad + e^{i\phi} \sin \phi_C \sin \theta_C \sin(\phi_T + \theta_T)|^2. \end{aligned} \quad (20)$$

Trivially, for $\phi = 0$ the controlled- U_ϕ gate reduces to a CNOT gate [16] and the polarization-dependent joint detection probability in Eq. (20) becomes

$$\begin{aligned}
 P_{\text{CNOT}} &:= |\langle \theta_C, \theta_T | \psi \rangle|^2 \\
 &= |\cos \phi_C \cos \theta_C \cos (\phi_T - \theta_T) \\
 &\quad + \sin \phi_C \sin \theta_C \sin (\phi_T + \theta_T)|^2.
 \end{aligned} \tag{21}$$

In order to simulate a controlled- U_ϕ gate we consider the interferometer in Fig.2. The interferometer consists of three parts: the first one prepares the initial polarization state in the “control” port \mathcal{C} and “target” port \mathcal{T} ; the second one implements polarization-dependent transformations along the control and target channels; the final part consists of the measurement process.

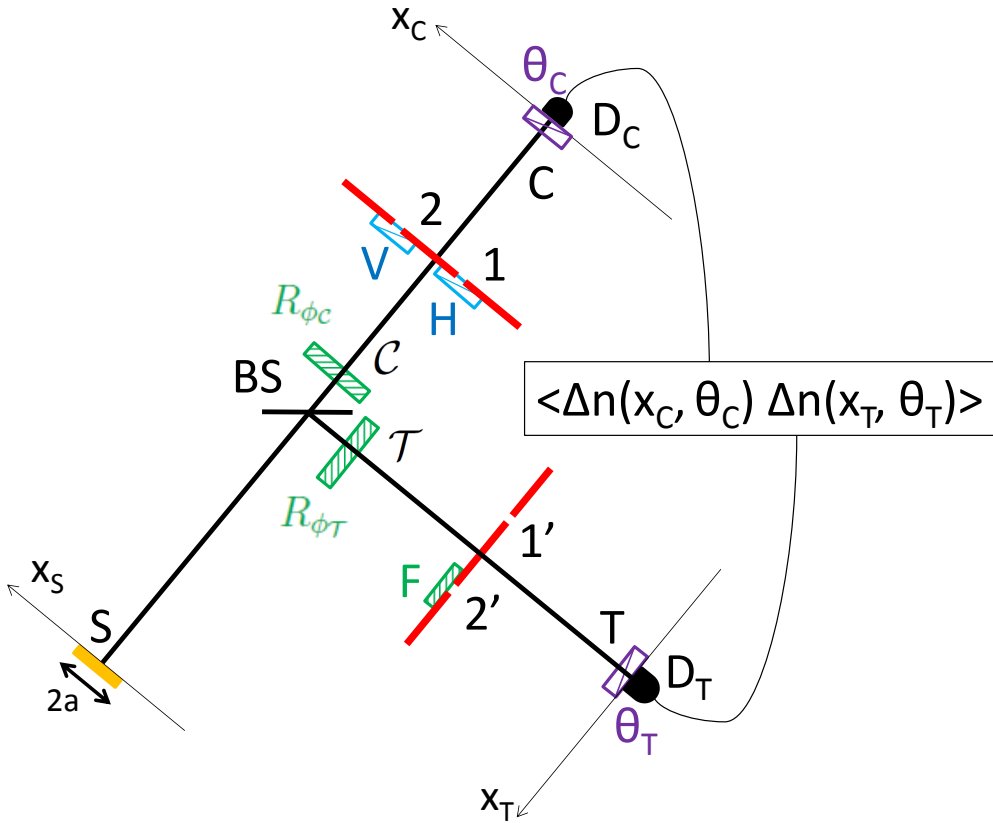


Figure 2. Interferometer for the simulation of controlled- U_ϕ gates. In the first part (from the source S to the ports \mathcal{C} and \mathcal{T}) of the interferometer, the initial polarization state of the light is prepared. The second part (from the ports \mathcal{C} and \mathcal{T} to the ports \mathcal{C} and \mathcal{T} , respectively) performs a polarization-dependent transformation. Correlation measurements in the fluctuations of the number of photons are finally performed at the interferometer output.

In the first part of the setup the H-polarized chaotic light first impinges on the beam-splitter and then propagates through two half-wave plates R_{ϕ_C} and R_{ϕ_T} , at the beam-

splitter output ports \mathcal{C} and \mathcal{T} . The chaotic light at the \mathcal{C} and \mathcal{T} ports is thus prepared in two arbitrary polarization states, along the direction $\phi_{\mathcal{C}}$ and $\phi_{\mathcal{T}}$, respectively.

The second part of the setup consists of a “control” path, connecting the ports \mathcal{C} and C , and a “target” path, connecting the ports \mathcal{T} and T . In the control path, analogously to the setup in Fig.1, the light goes through a two-pinholes mask. However, here, two polarizers along the H and V directions are placed just before the slits 1 and 2, respectively. In the target path, an identical two-pinholes mask is placed at the same distance from the beam splitter. Differently from the setup in Fig.2, a half-wave plate, with axis rotated by $\pi/4$ with respect to the H direction, is put in correspondence of the pinhole $2'$.

Let us finally describe the detection process. A polarizer, defined by the polarization $\theta_d := (\cos \theta_d \quad \sin \theta_d)^T$, with $d = C, T$, is placed just in front of each detector. The measurement consists of a polarization-dependent correlation measurement in the fluctuations of the number of photons $\Delta n(x_C, \theta_C)$ and $\Delta n(x_T, \theta_T)$.

Setting again for simplicity $x_C = x_T = 0$, and in the conditions (5) and (6), the expectation value of the product of the fluctuations of the number of photons reads ‡

$$\begin{aligned} & \langle \Delta n(0, \theta_C) \Delta n(0, \theta_T) \rangle \\ & \propto \left| G_{1,1'}^{(1)}(0, \theta_C, 0, \theta_T) + G_{2,2'}^{(1)}(0, \theta_C, 0, \theta_T) \right|^2 \\ & \propto P_{U_\phi}. \end{aligned} \quad (22)$$

Here, we find again two interfering contributions, $G_{1,1'}^{(1)}$ and $G_{2,2'}^{(1)}$, associated with the propagation through the two pairs of point-like slits $(1, 1')$ and $(2, 2')$, respectively. However, differently from the setup in Fig.1, these interfering contributions are now polarization dependent. Interestingly, the resulting interfering pattern is proportional to the probability P_{U_ϕ} in Eq.(20), associated with a controlled- U_ϕ gate, with ϕ defined in Eq.(17). When

$$|\phi(x_1, x_2, x_{1'}, x_{2'})| \ll 1, \quad (23)$$

Eq. (22) reduces to

$$\langle \Delta n(0, \theta_C) \Delta n(0, \theta_T) \rangle \propto P_{CNOT}, \quad (24)$$

with P_{CNOT} defined in Eq.(21), leading to the simulation of the CNOT gate operation. The condition (23) can be experimentally obtained, for example, by the condition

$$|x_{i'}^2 - x_i^2| \ll \frac{2l_{coh}an}{\pi z}, \quad (25)$$

for $i = 1, 2$, and with $l_{coh} = \lambda z / (2a)$.

4. Toward higher order correlations

The physical phenomena described in the previous section, can, in principle, be generalized in order to simulate higher-order entanglement correlations. Here, we

‡ See appendix [Appendix C](#) for a detailed demonstration.

introduce, in Fig.3, a modified setup analogous to the one introduced in the temporal domain in [10]. Indeed, interferometers of this type can be used to simulated higher-order network using the same technique developed in [10]. We demonstrate now how the interferometer in Fig.3 can also simulate a controlled- U_ϕ gate and, in particular, a CNOT gate.

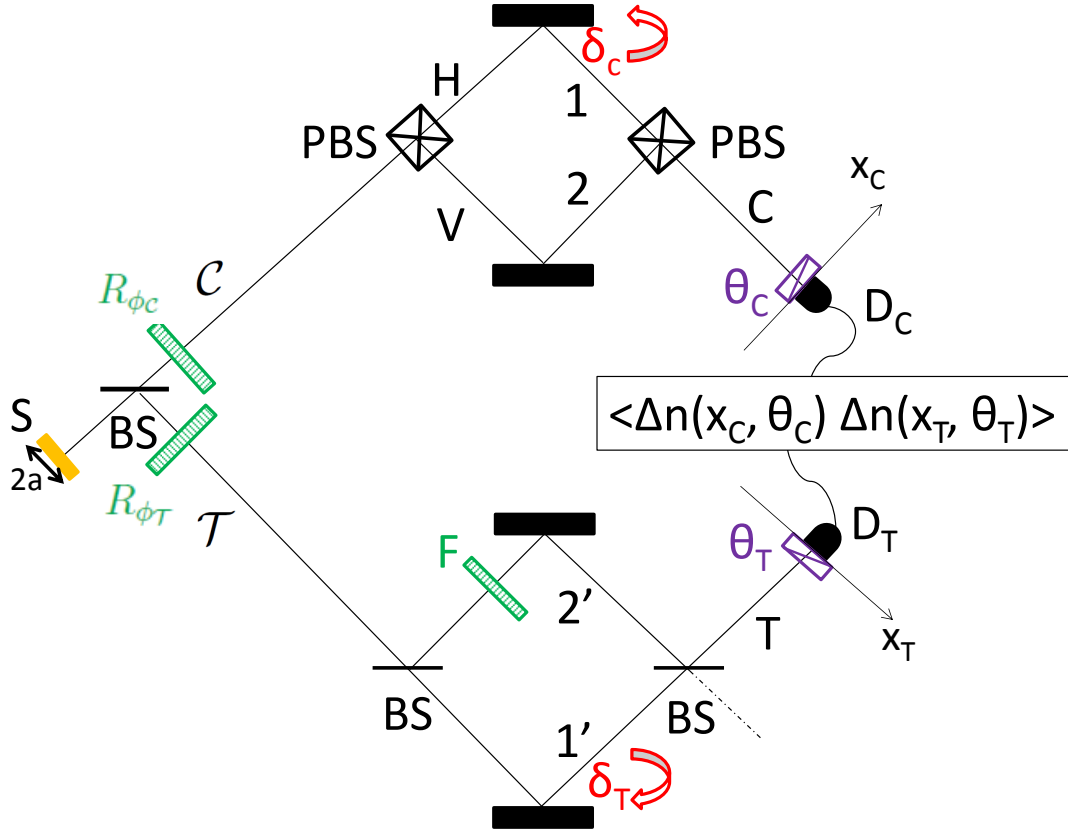


Figure 3. Modified interferometer for the simulation of controlled- U_ϕ gates which can be used as a building block for the implementation of more complex higher-order networks [10].

Here, the two masks in Fig.3 are substituted by two Mach-Zehnder interferometers: the “control” interferometer, connecting the port \mathcal{C} with the port \mathcal{C} , and the “target” interferometer, connecting the port \mathcal{T} with the port \mathcal{T} .

The control interferometer consists of two polarizing beam splitters and two tiltable mirrors. The mirror in one path is tilted by an angle δ_C , in the interferometer plane, with respect to the position ($\delta_C = 0$) corresponding to interferometric paths 1 and 2 of equal length.

In the target interferometer, the polarizing beam splitters are substituted by balanced non-polarizing beam splitters. Moreover, a half wave plate F (analogously to the setup in Fig.2), implementing a flip in polarization, is introduced along the path $2'$. Here, the tilting angle δ_T of the mirror determines the difference between the optical paths $1'$ and $2'$. The tilting angles δ_C and δ_T satisfy, in the small angle approximation,

the conditions

$$|\delta_d| \gg \frac{l_{coh}}{2\bar{z}}, \quad (26)$$

$$|\delta_C - \delta_T| \ll \frac{l_{coh}}{2\bar{z}}, \quad (27)$$

analogous to the conditions (5) and (6) where l_{coh} is the transverse coherence length of the source, and \bar{z} is the longitudinal length from the mirrors to the detectors.

Finally, correlations in the fluctuation of the number of photons are measured at the detector D_C and D_T , placed at the same longitudinal distance z from the source.

In the condition

$$|x_C - x_T| \ll l_{coh}, \quad (28)$$

we obtain the expectation value of the product of the photon-number fluctuations §

$$\begin{aligned} & \langle \Delta n(x_C, \theta_C) \Delta n(x_T, \theta_T) \rangle \\ & \propto \left| G_{1,1'}^{(1)}(x_C, \theta_C; x_T, \theta_T) + G_{2,2'}^{(1)}(x_C, \theta_C; x_T, \theta_T) \right|^2 \\ & \propto P_{U_{\phi(x_C, x_T, \delta_C, \delta_T)}}, \end{aligned} \quad (29)$$

where $P_{U_{\phi(x_C, x_T, \delta_C, \delta_T)}}$ is defined in Eq.(20), with

$$\phi(x_C, x_T, \delta_C, \delta_T) = \frac{2\omega}{cz} [\bar{z}^2(\delta_C^2 - \delta_T^2) + \bar{z}(x_C\delta_C - x_T\delta_T)]. \quad (30)$$

Here, analogously to the setup in Fig.2, the interference between the two pairs of paths (1, 1') and (2, 2') leads to the simulation of a controlled- U_ϕ operation, with U_ϕ defined in Eq(18). Also in this case the operation of a CNOT gate can be simulated if

$$|\phi(x_C, x_T, \delta_C, \delta_T)| \ll 1, \quad (31)$$

that can be achieved experimentally, for example, for

$$|\delta_C^2 - \delta_T^2| \ll \frac{l_{coh}a}{2\bar{z}^2\pi}, \quad (32)$$

and

$$|x_C\delta_C - x_T\delta_T| \ll \frac{l_{coh}a}{2\bar{z}\pi}. \quad (33)$$

with $l_{coh} = \lambda z / (2a)$.

5. Discussions

In this paper we theoretically demonstrated a second-order spatial interference effect emerging from correlation measurements in the photon-number fluctuations. We showed how interference between two pairs of correlated paths, associated with the slit pairs

§ See appendix [Appendix E](#) for a detailed demonstration.

(1, 1') and (2, 2') in the setup in Fig.1), occurs even if the the two pinhole pairs correspond to two coherence areas separated much further than the transverse coherent length l_{coh} of the source. Interestingly, the indistinguishability between the paths configurations (1, 1') and (2, 2') arises from the fact that the two correlated paths 1 and 1' (or 2 and 2') in the first (or second) pair have equal transverse optical lengths with respect to the source coherence length, independently of how far apart from each other are the optical lengths for one pair with respect to the other. Furthermore, we showed that the resulting interference pattern contain information simultaneously on the exact position of the four slits, which could have not retrieved by performing first order interference measurements separately at the two interferometric output channels. Therefore, this effect may have future important applications in high-precision metrology and imaging.

In addition, we demonstrated how this novel spatial interference phenomenon can be used (see Fig.2) to simulate a particular class of controlled- U_ϕ gates. This includes the simulation of a CNOT gate, which was recently obtained experimentally [32].

Finally, we introduced a modified setup (see Fig.2) for CNOT-gate simulations which can be used as a building block for more complex higher-order interferometric networks. Here, arbitrary-order entanglement correlations can be simulated on demand for potential applications in metrology as well as for the implementation of novel optical algorithms.

In conclusion, beyond the avenue of all possible applications, this spatial interference phenomenon provides, together with its temporal counterpart [10], a deeper understanding of the physics of coherence and multi-photon interference with a thermal source.

Acknowledgments

Appendix A. Calculation of the Green's function for the setup in Fig.(1)

Let us calculate explicitly the Green's propagator for the setup shown in Fig.1. We have [13, 36, 37]

$$\begin{aligned}
 g\{\kappa; S, x_d\} &= \frac{1}{\sqrt{2}} e^{i\varphi(d)} \int dx_s dx_M A(x_s) M(x_M) \\
 &\times e^{i\kappa x_s} \left\{ \frac{-i\omega}{2\pi c} \frac{e^{i\omega z/c}}{z} \mathcal{G}(|x_s - x_M|)_{[\omega/(cz)]} \right\} \\
 &\times \left\{ \frac{-i\omega}{2\pi c} \frac{e^{i\omega \frac{f}{c}}}{f} \mathcal{G}(|x_M - x_d|)_{[\omega/(cf)]} \right\},
 \end{aligned} \tag{A.1}$$

where $A(x_s)$ is the source amplitude profile, $M(x_M)$ is the mask transfer function defined for simplicity by

$$M(x_M) := \sum_j \delta(x_M - x_j), \tag{A.2}$$

with $j = 1, 2$ for the upper mask and $j = 1', 2'$, for the lower mask, $\mathcal{G}(|\alpha|)_{[\beta]}$ is the Fresnel propagator

$$\mathcal{G}(|\alpha|)_{[\beta]} = e^{i\frac{\beta}{2}|\alpha|^2} \quad (\text{A.3})$$

and the factor $\frac{1}{\sqrt{2}}e^{i\varphi(d)}$ takes into account the propagation through the beam-splitter, with the assumption that $\varphi(C) = 0$ for the transmitted ray and $\varphi(D) = \pi$ for the reflected ray \parallel . Let us remind the properties of the Fresnel propagator:

$$\begin{aligned} \mathcal{G}^*(|\alpha|)_{[\beta]} &= \mathcal{G}(|\alpha|)_{[-\beta]} \\ \mathcal{G}(|\alpha + \alpha'|)_{[\beta]} &= \mathcal{G}(|\alpha|)_{[\beta]}\mathcal{G}(|\alpha'|)_{[\beta']}e^{i\beta\alpha\alpha'}. \end{aligned} \quad (\text{A.4})$$

Substituting the second property of Eq.(A.4) in Eq.(A.1), we have

$$\begin{aligned} g\{\kappa; S, x_d\} &= -\frac{1}{\sqrt{2}}e^{i\varphi(d)} \left(\frac{\omega}{2\pi c}\right)^2 \frac{e^{i\omega(z+f)/c}}{zf} \\ &\times \int dx_s dx_M A(x_s)M(x_M)e^{i\kappa x_s}\mathcal{G}(|x_s|)_{[\omega/(cz)]} \\ &\times \mathcal{G}(|x_M|)_{[\omega/(cz)]}e^{-i\omega x_s x_M/(zc)}\mathcal{G}(|x_M|)_{[\omega/(cf)]} \\ &\times \mathcal{G}(|x_d|)_{[\omega/(cf)]}e^{-i\omega x_d x_M/(fc)}. \end{aligned} \quad (\text{A.5})$$

Now substituting the first property of Eq.(A.4) in Eq.(A.5) and rearranging the result, we obtain

$$\begin{aligned} g\{\kappa; S, x_d\} &= -\frac{1}{\sqrt{2}} \left(\frac{\omega}{2\pi c}\right)^2 \frac{e^{i[\varphi(d)+\omega(z+f)/c]}}{zf} \\ &\times \mathcal{G}(|x_d|)_{[\omega/(cf)]} \\ &\times \int dx_M M(x_M)\mathcal{G}(|x_M|)_{[\omega/(cn)]}e^{-i\omega x_d x_M/(fc)} \\ &\times \int dx_s A(x_s)\mathcal{G}(|x_s|)_{[\omega/(cz)]}e^{i[\kappa-\omega x_M/(zc)]x_s}, \end{aligned} \quad (\text{A.6})$$

where

$$\frac{1}{n} = \frac{1}{z} + \frac{1}{f}. \quad (\text{A.7})$$

Considering the mask transfer function (Eq.(A.2)), Eq.(A.6) becomes

$$\begin{aligned} g\{\kappa; S, x_d\} &= \sum_j B_j(x_d) \int dx_s A(x_s)\mathcal{G}(|x_s|)_{[\omega/(cz)]} \\ &\times e^{i[\kappa-\omega x_j/(zc)]x_s}, \end{aligned} \quad (\text{A.8})$$

where

$$\begin{aligned} B_j(x_d) &= -\frac{1}{\sqrt{2}} \left(\frac{\omega}{2\pi c}\right)^2 \frac{e^{i[\varphi(d)+\omega(z+f)/c]}}{zf} \mathcal{G}(|x_d|)_{[\omega/(cf)]} \\ &\times \mathcal{G}(|x_j|)_{[\omega/(cn)]}e^{-i\omega x_d x_j/(fc)}. \end{aligned} \quad (\text{A.9})$$

\parallel A more formal calculation will be done in the appendix [Appendix C](#), taking into account the beam-splitter matrix.

Eq.(A.8) shows that the Green's function is the summation of two contributions, one from each point-like aperture in the mask:

$$g\{\kappa; S, x_d\} = \sum_j g_j\{\kappa; S, x_d\}, \quad (\text{A.10})$$

with

$$g_j\{\kappa; S, x_d\} = B_j(x_d) \int dx_s A(x_s) \mathcal{G}(|x_s|)_{[\omega/(cz)]} \\ \times e^{i[\kappa - \omega x_j/(zc)]x_s}, \quad (\text{A.11})$$

Green's function from the source S to the detector D_d , through the point-like aperture j .

Appendix B. Calculation of the correlation function for the setup in Fig.1.

In the present appendix we present a detailed calculation to obtain Eq.s (12) and (16).

By substituting in Eq.(9) the result obtained by inserting the Green's function given by Eq.(A.10) and (A.11) into the electric field given by Eq.(10) and Eq.(11), we obtain:

$$G^{(1)}(x_C, x_T) = \sum_{\substack{i=1,2 \\ j=1',2'}} |K|^2 Tr \left[\hat{\rho}_H \int d\kappa d\kappa' \right. \\ \left. \times g_i^*\{\kappa; S, x_C\} g_j\{\kappa'; S, x_T\} \hat{a}_s^+(\kappa) \hat{a}_s(\kappa') \right], \quad (\text{B.1})$$

where $K = \iota \sqrt{\frac{\hbar\omega}{2\epsilon_0}}$. We can define the pairs of paths as

$$G_{i,j}^{(1)}(x_C, x_T) = |K|^2 Tr \left[\hat{\rho}_H \int d\kappa d\kappa' \right. \\ \left. \times g_i^*\{\kappa; S, x_C\} g_j\{\kappa'; S, x_T\} \hat{a}_s^+(\kappa) \hat{a}_s(\kappa') \right]. \quad (\text{B.2})$$

in such a way that Eq.(B.1) can be written as:

$$G^{(1)}(x_C, x_T) = \sum_{\substack{i=1,2 \\ j=1',2'}} G_{i,j}^{(1)}(x_C, x_T). \quad (\text{B.3})$$

By using the property of chaotic sources [34]

$$Tr [\hat{\rho} a^+(\kappa) a(\kappa')] = \langle n_\kappa \rangle \delta(\kappa - \kappa'), \quad (\text{B.4})$$

Eq.(B.2) reduces to

$$G_{i,j}^{(1)}(x_C, x_T) = K' \int d\kappa g_i^*\{\kappa; S, x_C\} g_j\{\kappa; S, x_T\}, \quad (\text{B.5})$$

with $K' = |K|^2 \langle n_\kappa \rangle$, and $\langle n_\kappa \rangle$ the average photon number in the mode κ , assumed to

be constant. By substituting in Eq.(B.5) the results of Eq.s (A.8, A.10), we get

$$\begin{aligned}
G_{i,j}^{(1)}(x_C, x_T) &= K' \int d\kappa g_i^* \{ \kappa; S, x_C \} g_j \{ \kappa; S, x_T \} \\
&= K' B_i^*(x_C) \int dx_s A^*(x_s) e^{i\omega x_i x_s / (cz)} \mathcal{G}^*(|x_s|)_{[\omega/(cz)]} \\
&\times B_j(x_T) \int dx'_s A(x'_s) e^{-i\omega x_j x'_s / (cz)} \mathcal{G}(|x'_s|)_{[\omega/(cz)]} \\
&\times \int d\kappa e^{i\kappa(x'_s - x_s)} \\
&= K' B_i^*(x_C) B_j(x_T) \int dx_s |A(x_s)|^2 e^{i\omega(x_i - x_j)x_s / (cz)} \\
&= K' B_i^*(x_C) B_j(x_T) FT \{ |A(x_s)|^2 \} [\omega(x_i - x_j) / (2\pi cz)],
\end{aligned} \tag{B.6}$$

where $FT \{ |A(x_s)|^2 \} [\chi]$ represents the Fourier transform of the source intensity profile, calculated in χ .

Setting for simplicity the source amplitude profile

$$A(x_s) := \begin{cases} 1 & |x_s| \leq a \\ 0 & |x_s| > a \end{cases}, \tag{B.7}$$

we have that

$$\begin{aligned}
&FT \{ |A(x_s)|^2 \} [\omega(x_i - x_j) / (2\pi cz)] \\
&= 2a \operatorname{sinc} [\pi(x_i - x_j) / l_{coh}],
\end{aligned} \tag{B.8}$$

where $l_{coh} = \lambda z / (2a)$.

Apart from a constant factor, the result shown in Eq.(B.6) would be the same yield by placing two point-like detectors in the positions x_i and x_j respectively. Using Eq.(B.8), we have that when $|x_i - x_j| > l_{coh}$, the Fourier transform of the source profile is approximately zero, revealing the absence of correlation between the intensities detected. On the contrary the correlation reaches its maximum value for $|x_i - x_j| \ll l_{coh}$. Based on the conditions (5) and (6), we have that the Fourier Transform is approximately zero, for the contributions coming from the apertures (1, 2') and (1', 2), while it is approximately equal to $FT \{ |A(x_s)|^2 \} (0)$ for the contributions coming from (1, 1') and (2, 2'). Therefore by inserting the conditions of (5) and (6) in Eq.(B.6), and substituting the result in Eq.(B.3) we get

$$G^{(1)}(x_C, x_T) = G_{1,1'}^{(1)}(x_C, x_T) + G_{2,2'}^{(1)}(x_C, x_T), \tag{B.9}$$

that, based on the definition in Eq.(8), gives the result shown in Eq.(12).

Based on Eq.s (5) and (6), and (B.6), the explicit expression of $G^{(1)}(x_C, x_T)$ is given by

$$\begin{aligned}
G^{(1)}(x_C, x_T) &= K' FT \{ |A(x_s)|^2 \} (0) \\
&\times [B_1^*(x_C) B_{1'}(x_T) + B_2^*(x_C) B_{2'}(x_T)].
\end{aligned} \tag{B.10}$$

By inserting the definition given in Eq.(A.9) we have

$$\begin{aligned} G^{(1)}(x_C, x_T) &= C_b \mathcal{G}^*(|x_C|)_{[\omega/(cz)]} \mathcal{G}(|x_T|)_{[\omega/(cz)]} \\ &\times \left[\mathcal{G}^*(|x_1|)_{[\omega/(cn)]} \mathcal{G}(|x_{1'}|)_{[\omega/(cn)]} e^{i\omega/(cf)(x_C x_1 - x_T x_{1'})} \right. \\ &\left. + \mathcal{G}^*(|x_2|)_{[\omega/(cn)]} \mathcal{G}(|x_{2'}|)_{[\omega/(cn)]} e^{i\omega/(cf)(x_C x_2 - x_T x_{2'})} \right], \end{aligned}$$

with $C_b = (\iota/2) [1/(zf)]^2 K' [\omega/(2\pi c)]^4 FT \{|A(x_s)|^2\} (0)$. By plugging in the above result in Eq.(8) we have

$$\begin{aligned} \langle \Delta n(x_C) \Delta n(x_T) \rangle &= C'_b \tag{B.11} \\ &\left| \mathcal{G}^*(|x_1|)_{[\omega/(cn)]} \mathcal{G}(|x_{1'}|)_{[\omega/(cn)]} e^{i\omega/(cf)(x_C x_1 - x_T x_{1'})} \right. \\ &\left. + \mathcal{G}^*(|x_2|)_{[\omega/(cn)]} \mathcal{G}(|x_{2'}|)_{[\omega/(cn)]} e^{i\omega/(cf)(x_C x_2 - x_T x_{2'})} \right|^2, \end{aligned}$$

where $C'_b = |C_b|^2$.

Let us simplify the situation by taking $x_C = x_T = 0$. Now based on the definition of the Fresnel propagator (Eq.(A.3)), we get

$$\begin{aligned} \langle \Delta n(0) \Delta n(0) \rangle &= C'_b \left| \mathcal{G}^*(|x_1|)_{[\omega/(cn)]} \mathcal{G}(|x_{1'}|)_{[\omega/(cn)]} \right. \\ &\left. + \mathcal{G}^*(|x_2|)_{[\omega/(cn)]} \mathcal{G}(|x_{2'}|)_{[\omega/(cn)]} \right|^2, \tag{B.12} \end{aligned}$$

in such a way that

$$\langle \Delta n(0) \Delta n(0) \rangle = C'_b \left| e^{i\omega/(2cn)(x_1^2 - x_1'^2)} + e^{i\omega/(2cn)(x_2^2 - x_2'^2)} \right|^2, \tag{B.13}$$

as in Eq.(16).

Appendix C. Calculation of the correlation function for the setup in Fig.2.

In the present appendix we present the detailed calculation to obtain Eq.(22).

As depicted in Fig.2, polarizers oriented at θ_C and θ_T are placed in front of detectors D_C and D_T , respectively. The polarization-dependent correlation between the fluctuations of the photon number, for quasi-monochromatic 1-dim chaotic sources ρ_S , is given by

$$\langle \Delta n(x_C, \theta_C) \Delta n(x_T, \theta_T) \rangle = |G^{(1)}(x_C, \theta_C; x_T, \theta_T)|^2, \tag{C.1}$$

where

$$\begin{aligned} G^{(1)}(x_C, \theta_C; x_T, \theta_T) &\tag{C.2} \\ &:= \text{tr} \left[\hat{\rho}_{S, S'} \left(\boldsymbol{\theta}_C \cdot \hat{\mathbf{E}}_C^{(-)}(x_C) \right) \left(\boldsymbol{\theta}_T \cdot \hat{\mathbf{E}}_T^{(+)}(x_T) \right) \right], \end{aligned}$$

is the polarization-dependent first-order correlation function, with $\hat{\rho}_{S, S'} = \hat{\rho}_S \otimes \hat{\rho}_{S'}$, the input state of the beam-splitter (with $\rho_{S'}$ the state of the source in the unused input port of the beam-splitter, not shown in Fig. 2, i.e. $\rho_{S'} = |0\rangle\langle 0|$), and

$$\hat{\mathbf{E}}_d^{(+)}(x_d) = \iota \sqrt{\frac{\hbar\omega}{2\epsilon_0}} \int d\kappa e^{-i\omega t} \begin{pmatrix} \hat{a}_d^H(\kappa) \\ \hat{a}_d^V(\kappa) \end{pmatrix}, \tag{C.3}$$

the positive frequency part of the electric field at the detector D_d , with $d = C, T$. The field in Eq.(C.3) has been written in the near field approximation and in the hypothesis that the detection time t is the same for both detectors; $\hat{a}_d^{(H)}(\kappa)$ and $\hat{a}_d^{(V)}(\kappa)$ represent the annihilation operators at the detector D_d associated with the H and V polarization modes, respectively, and with the component of the transverse wave vector κ . In Eq.(C.2), $\hat{\mathbf{E}}_d^{(-)}(x_d)$ is the Hermitian conjugate of the Eq.(C.3). The electric field defined in Eq.(C.3) can also be written as the sum of the contributions coming from the sources S and S' , namely:

$$\hat{\mathbf{E}}_d^{(+)}(x_d) = \sum_{s=S,S'} \hat{\mathbf{E}}_{d,s}^{(+)}(x_d), \quad (\text{C.4})$$

where

$$\hat{\mathbf{E}}_{d,s}^{(+)}(x_d) = \iota \sqrt{\frac{\hbar\omega}{2\epsilon_0}} \int d\kappa e^{-i\omega t} \mathcal{M}_{d,s}(\kappa) \begin{pmatrix} \hat{a}_s^H(\kappa) \\ \hat{a}_s^V(\kappa) \end{pmatrix} \quad (\text{C.5})$$

is the electric field operator at the detector D_d , written in terms of the annihilation operators $\hat{a}_s^{(H)}(\kappa)$ and $\hat{a}_s^{(V)}(\kappa)$ associated with the input port s of the beam-splitter; $\mathcal{M}_{d,s}(\kappa)$ is the matrix describing the propagation from the source s , to the detector D_d for the mode κ .

As depicted in Fig.2, we suppose the chaotic ρ_S be H-polarized; we thus indicate it as ρ_H . In this hypothesis, Eq.(C.2) reduces to

$$G^{(1)}(x_C, \theta_C; x_T, \theta_T) := \text{Tr} \left[\hat{\rho}_H \hat{\mathcal{E}}_{C,S}^-(x_C) \hat{\mathcal{E}}_{T,S}^+(x_T) \right], \quad (\text{C.6})$$

with

$$\hat{\mathcal{E}}_{d,S}^+(x_d) := K \boldsymbol{\theta}_d \cdot \left[\int d\kappa e^{-i\omega t} \mathcal{M}_{d,S}(\kappa) \begin{pmatrix} \hat{a}_S^H(\kappa) \\ 0 \end{pmatrix} \right], \quad (\text{C.7})$$

where $K = \iota \sqrt{\frac{\hbar\omega}{2\epsilon_0}}$. By defining

$$L_d(\kappa) := (\cos \theta_d \quad \sin \theta_d) \mathcal{M}_{d,S}(\kappa) \begin{pmatrix} 1 \\ 0 \end{pmatrix}, \quad (\text{C.8})$$

Eq.(C.7) can be rewritten as:

$$\hat{\mathcal{E}}_{d,S}^+(x_d) = K \int d\kappa e^{-i\omega t} L_d(\kappa) \hat{a}_S^H(\kappa), \quad (\text{C.9})$$

and Eq.(C.6) becomes:

$$\begin{aligned} G^{(1)}(x_C, \theta_C; x_T, \theta_T) &= |K|^2 \text{Tr} \left[\hat{\rho}_H \int d\kappa d\kappa' L_C^*(\kappa) L_T(\kappa') \right. \\ &\quad \left. \times \hat{a}_S^{+H}(\kappa) \hat{a}_S^H(\kappa') \right] \\ &= K' \int d\kappa L_C^*(\kappa) L_T(\kappa), \end{aligned} \quad (\text{C.10})$$

where we have used the property given in Eq.(B.4).

We calculate $L_C(\kappa)$ and $L_T(\kappa)$, by using the propagation matrices $\mathcal{M}_{d,S}(\kappa)$ (with $d = C, T$), obtained in Appendix D (Eq.(D.12)):

$$\begin{aligned} L_C(\kappa) &:= (\cos \theta_C \quad \sin \theta_C) \mathcal{P}_{C,C}(\kappa) R_{\phi_C} g\{\kappa; S, R_{\phi_C}\} \begin{pmatrix} 1 \\ 0 \end{pmatrix}, \\ L_T(\kappa) &:= (\cos \theta_T \quad \sin \theta_T) \mathcal{P}_{T,T}(\kappa) R_{\phi_T} g\{\kappa; S, R_{\phi_T}\} \begin{pmatrix} 1 \\ 0 \end{pmatrix}, \end{aligned} \tag{C.11}$$

Now by employing the results of Eq.s (D.5), (D.7), (D.8), (D.9) and (D.10), and the property given in Eq.(D.11), we get:

$$\begin{aligned} L_C(\kappa) &= \frac{1}{\sqrt{2}} [g_1\{\kappa; S, x_C\} \cos \theta_C \cos \phi_C \\ &\quad + g_2\{\kappa; S, x_C\} \sin \theta_C \sin \phi_C] \end{aligned} \tag{C.12}$$

and

$$\begin{aligned} L_T(\kappa) &= \frac{\imath}{\sqrt{2}} [g_{1'}\{\kappa; S, x_T\} \cos(\theta_T - \phi_T) \\ &\quad + g_{2'}\{\kappa; S, x_T\} \sin(\theta_T + \phi_T)], \end{aligned} \tag{C.13}$$

with

$$\begin{aligned} g_p\{\kappa; S, x_d\} &= - \left(\frac{\omega}{2\pi c} \right)^2 \frac{e^{\imath[\omega(z+f)/c]}}{zf} \mathcal{G}(|x_d|)_{[\omega/(cf)]} \\ &\quad \times \mathcal{G}(|x_p|)_{[\omega/(cn)]} e^{-\imath\omega x_d x_p / (fc)} \\ &\quad \times \int dx_s A(x_s) \mathcal{G}(|x_s|)_{[\omega/(cz)]} \\ &\quad \times e^{\imath[\kappa - \omega x_p / (zc)] x_s}, \end{aligned} \tag{C.14}$$

the Green's function describing the propagation of the mode κ from the source S to the point x_d in the plane of the detector D_d , going through the aperture $p = 1, 2, 1', 2'$. Plugging in the results in Eq.s (C.12) and (C.13), the correlation function of Eq.(C.10) becomes

$$\begin{aligned} G^{(1)}(x_C, \theta_C; x_T, \theta_T) & \tag{C.15} \\ &= \frac{\imath}{2} K' \int d\kappa \\ &\quad \times [\cos \theta_C \cos \phi_C \cos(\theta_T - \phi_T) g_1\{\kappa; S, x_C\} g_{1'}^*\{\kappa; S, x_T\} \\ &\quad + \sin \theta_C \sin \phi_C \sin(\theta_T + \phi_T) g_2\{\kappa; S, x_C\} g_{2'}^*\{\kappa; S, x_T\} \\ &\quad - \cos \theta_C \cos \phi_C \sin(\theta_T + \phi_T) g_1\{\kappa; S, x_C\} g_{2'}^*\{\kappa; S, x_T\} \\ &\quad - \sin \theta_C \sin \phi_C \cos(\theta_T - \phi_T) g_2\{\kappa; S, x_C\} g_{1'}^*\{\kappa; S, x_T\}], \end{aligned}$$

with $K' = |K|^2 \langle n_\kappa \rangle$. To obtain the result shown in Eq.(22), we insert Eq.(C.15) into Eq.(C.1) after:

a inserting Eq.(C.14) in Eq.(C.15),

- b carrying on a calculation similar to the one in Eq.(B.6),
- c employing the conditions given in Eq.s (5) and (6),
- d simplifying the result by taking $x_C = x_T = 0$.

We get:

$$\begin{aligned}
& \langle \Delta n(0, \theta_C) \Delta n(0, \theta_T) \rangle \\
&= C'_b \left| e^{i\omega/(2cn)(x_1'^2 - x_1^2)} \cos \theta_C \cos \phi_C \cos(\theta_T - \phi_T) \right. \\
&\quad \left. + e^{i\omega/(2cn)(x_2'^2 - x_2^2)} \sin \theta_C \sin \phi_C \sin(\theta_T + \phi_T) \right|^2,
\end{aligned} \tag{C.16}$$

where $C'_b = |(\iota/2) [1/(zf)]^2 K' [\omega/(2\pi c)]^4 FT \{|A(x_s)|^2\} (0)|^2$.

Appendix D. Calculation of the propagation matrix $\mathcal{M}(\kappa)$

In this appendix we calculate the propagation matrix $\mathcal{M}_{d,S}(\kappa)$ introduced in Eq.(C.5).

In the setup of Fig.2, the propagation from the sources (S, S') to the beam-splitter can be written in matrix form as:

$$P_{ini}(\kappa) := \begin{pmatrix} g\{\kappa; S, BS\} \mathbb{1} & 0 \\ 0 & g\{\kappa; S', BS\} \mathbb{1} \end{pmatrix}, \tag{D.1}$$

where $g\{\kappa; s, BS\}$ is the Green's function propagator in the mode κ from the source s to the beam-splitter, with $s = S, S'$; the matrix associated with the beam-splitter is

$$BS := \frac{1}{\sqrt{2}} \begin{pmatrix} \mathbb{1} & \iota \mathbb{1} \\ \iota \mathbb{1} & \mathbb{1} \end{pmatrix}. \tag{D.2}$$

The propagation from the beam-splitter to the half-wave plates (R_{ϕ_C}, R_{ϕ_T}) is described by

$$P_1(\kappa) := \begin{pmatrix} g\{\kappa; BS, R_{\phi_C}\} \mathbb{1} & 0 \\ 0 & g\{\kappa; BS, R_{\phi_T}\} \mathbb{1} \end{pmatrix}, \tag{D.3}$$

where $g\{\kappa; BS, R_{\phi_i}\}$ is the Green's function propagating the mode κ from beam-splitter to the half-wave plate R_{ϕ_i} with $i = C, T$. The matrix describing the propagation through both of the half-wave plates is

$$\mathcal{R} := \text{diag}(R_{\phi_C}, R_{\phi_T}), \tag{D.4}$$

where

$$R_{\phi_i} := \begin{pmatrix} \cos \phi_i & \sin \phi_i \\ \sin \phi_i & -\cos \phi_i \end{pmatrix}, \tag{D.5}$$

with $i = C, T$. The propagation from the half-wave plates R_{ϕ_C} and R_{ϕ_T} to the detectors points x_C and x_T defined, respectively, on the plane of the detectors D_C and D_T is described by

$$P_2(\kappa) := \begin{pmatrix} \mathcal{P}_{C,C}(\kappa) & 0 \\ 0 & \mathcal{P}_{T,T}(\kappa) \end{pmatrix}, \tag{D.6}$$

where

$$\begin{aligned}\mathcal{P}_{C,C}(\kappa) &:= \int dx_M g\{\kappa; R_{\phi_C}, x_M\} \tilde{M}_C(x_M) g\{\kappa; x_M, x_C\}, \\ \mathcal{P}_{T,T}(\kappa) &:= \int dx_M g\{\kappa; R_{\phi_T}, x_M\} \tilde{M}_T(x_M) g\{\kappa; x_M, x_T\},\end{aligned}\tag{D.7}$$

with $g\{\kappa; R_{\phi_i}, x_M\}$ the Green's function propagating the mode κ from the half-wave plate R_{ϕ_i} to the point x_M , defined in the plane of the mask, $g\{\kappa; x_M, x_d\}$ the Green's function from the point x_M of the mask to the detector D_d , and

$$\begin{aligned}\tilde{M}_C(x_M) &:= \delta(x_M - x_1)P_H + \delta(x_M - x_2)P_V, \\ \tilde{M}_T(x_M) &:= \delta(x_M - x_{1'})\mathbb{1} + \delta(x_M - x_{2'})F,\end{aligned}\tag{D.8}$$

the overall transmission functions of the masks placed, respectively, in the arm C and T of the setup, which take into account both the mask transfer functions (Eq.(A.2), the polarizers

$$P_H := \begin{pmatrix} 1 & 0 \\ 0 & 0 \end{pmatrix}, P_V := \begin{pmatrix} 0 & 0 \\ 0 & 1 \end{pmatrix},\tag{D.9}$$

and the half-wave plate

$$F := \begin{pmatrix} 0 & 1 \\ 1 & 0 \end{pmatrix}\tag{D.10}$$

placed on the mask (see Fig.2). By using the property of the Green's function:

$$g\{\kappa; a, b\}g\{\kappa; b, x_d\} = g\{\kappa; a, x_d\},\tag{D.11}$$

and Eq.s (D.1), (D.2), (D.3), (D.4), (D.6), we obtain that the propagation from the sources (S,S') to the detectors is given by

$$\begin{aligned}\mathcal{M}(\kappa) &:= P_2(\kappa)\mathcal{R} P_1(\kappa) BS P_{ini}(\kappa) = \frac{1}{\sqrt{2}} \\ &\times \begin{pmatrix} \mathcal{P}_{C,C}(\kappa)R_{\phi_C}g\{\kappa; S, R_{\phi_C}\} & i\mathcal{P}_{C,C}(\kappa)R_{\phi_C}g\{\kappa; S', R_{\phi_C}\} \\ i\mathcal{P}_{T,T}(\kappa)R_{\phi_T}g\{\kappa; S, R_{\phi_T}\} & \mathcal{P}_{T,T}(\kappa)R_{\phi_T}g\{\kappa; S', R_{\phi_T}\} \end{pmatrix} \\ &= \begin{pmatrix} \mathcal{M}_{C,S}(\kappa) & \mathcal{M}_{C,S'}(\kappa) \\ \mathcal{M}_{T,S}(\kappa) & \mathcal{M}_{T,S'}(\kappa) \end{pmatrix},\end{aligned}\tag{D.12}$$

where $g\{\kappa; s, R_{\phi_i}\}$ is the Green's function propagating the mode κ from the source $s = S, S'$, to the half-wave plate R_{ϕ_i} , with $i = C, T$.

Appendix E. Calculation of the correlation function for the setup in Fig.3

In the present appendix we present the detailed calculation to obtain Eq.(29).

In the setup depicted in Fig.3, we label as S' the source in the unused input port to the beam splitter (not shown in the Figure), and consider the following conditions:

- (A) $\hat{\rho}_{S'} = |vac\rangle\langle vac|$,
- (B) $\hat{\rho}_S$ is H-polarized,
- (C) the tilting angles δ_d , with $d = C, T$, are defined in the plane of the interferometer.

The first order correlation function is still given by Eq.(C.10), with $L_d(\kappa)$ replaced by

$$L'_d(\kappa) := (\cos \theta_d \quad \sin \theta_d) \mathcal{M}'_{d,S}(\kappa) \begin{pmatrix} 1 \\ 0 \end{pmatrix}, \quad (\text{E.1})$$

for $d = C, T$, $\mathcal{M}'_{d,S}(\kappa)$ is the matrix describing the propagation of the transverse mode κ , from the source S , to the detector D_d , in the setup of Fig.3.

We calculate $L'_C(\kappa)$ and $L'_T(\kappa)$, by using the propagation matrices $\mathcal{M}'_{d,S}(\kappa)$ (with $d = C, T$), obtained in Appendix F (Eq.(F.5)):

$$\begin{aligned} L'_C(\kappa) &:= (\cos \theta_C \quad \sin \theta_C) \mathcal{P}'_{C,C}(\kappa) R_{\phi_C} g\{\kappa; S, R_{\phi_C}\} \begin{pmatrix} 1 \\ 0 \end{pmatrix}, \\ L'_T(\kappa) &:= (\cos \theta_T \quad \sin \theta_T) {}_i\mathcal{P}'_{T,T}(\kappa) R_{\phi_T} g\{\kappa; S, R_{\phi_T}\} \begin{pmatrix} 1 \\ 0 \end{pmatrix}. \end{aligned} \quad (\text{E.2})$$

Now by employing the results of Eq.s (D.5), (D.10), (F.3) and (F.4), and the property given in Eq.(D.11), we get:

$$\begin{aligned} L'_C(\kappa) &= \frac{\imath}{\sqrt{2}} \\ &\times [g_1\{\kappa; S, x_C\} \cos \theta_C \cos \phi_C - g_2\{\kappa; S, x_C\} \sin \theta_C \sin \phi_C] \end{aligned} \quad (\text{E.3})$$

and

$$\begin{aligned} L'_T(\kappa) &= -\frac{1}{2\sqrt{2}} \\ &\times [g_{1'}\{\kappa; S, x_T\} \cos(\theta_T - \phi_T) - g_{2'}\{\kappa; S, x_T\} \sin(\theta_T + \phi_T)]. \end{aligned} \quad (\text{E.4})$$

Plugging in the results in Eq.s (E.3) and (E.4), the correlation function of Eq.(C.10) (replacing $L_d(\kappa)$ with $L'_d(\kappa)$, with $d = C, T$), becomes

$$\begin{aligned} G^{(1)}(x_C, \theta_C; x_T, \theta_T) & \\ &= K' \int d\kappa L_C^*(\kappa) L'_T(\kappa) = \frac{\imath}{4} K' \int d\kappa \\ &\times [\cos \theta_C \cos \phi_C \cos(\theta_T - \phi_T) g_1\{\kappa; S, x_C\} g_{1'}^*\{\kappa; S, x_T\} \\ &+ \sin \theta_C \sin \phi_C \sin(\theta_T + \phi_T) g_2\{\kappa; S, x_C\} g_{2'}^*\{\kappa; S, x_T\} \\ &- \cos \theta_C \cos \phi_C \sin(\theta_T + \phi_T) g_1\{\kappa; S, x_C\} g_{2'}^*\{\kappa; S, x_T\} \\ &- \sin \theta_C \sin \phi_C \cos(\theta_T - \phi_T) g_2\{\kappa; S, x_C\} g_{1'}^*\{\kappa; S, x_T\}], \end{aligned} \quad (\text{E.5})$$

with $K' = |K|^2 \langle n_\kappa \rangle$. In the small angle approximation for δ_C, δ_T , we have

$$\begin{aligned} g_p\{\kappa; S, x_d\} &= \frac{-\imath\omega e^{\imath\omega z/c}}{2\pi c} \frac{1}{z} \\ &\times \int dx_S A(x_S) e^{-\imath\kappa x_S} e^{-\imath\omega(x_S - x_{d,p})^2/(2zc)}, \end{aligned} \quad (\text{E.6})$$

where $x_{d,p}$ is the detector D_d “effective” transverse position, determined by the p -path ($p = 1, 2, 1', 2'$); for the four cases, we have: $x_{C,2} = x_C$, $x_{T,2'} = x_T$, $x_{C,1} = x_C + 2\bar{z}\delta_C$ and $x_{T,1'} = x_T + 2\bar{z}\delta_T$, with \bar{z} the longitudinal distance from the mirrors to the detectors. Each term in Eq.(E.5) gives

$$\begin{aligned} & \int d\kappa g_i^* \{\kappa; S, x_C\} g_j \{\kappa; S, x_T\} \\ & \propto \int d\kappa dx_S dx'_S A^*(x_S) A(x'_S) \\ & \times e^{-i\kappa(x'_S - x_S)} e^{-i\omega/(2zc) [(x'_S - x_{T,j})^2 - (x_S - x_{C,i})^2]} \\ & = e^{i\omega(x_{C,i}^2 - x_{T,j}^2)/(2zc)} FT \{ |A(x_S)|^2 \} [\omega(x_{T,j} - x_{C,i})/(2\pi zc)], \end{aligned} \quad (\text{E.7})$$

where $FT \{ |A(x_S)|^2 \} [\omega(x_{T,j} - x_{C,i})/(2\pi zc)]$ represents the Fourier transform of the source intensity profile calculated in $\omega(x_{T,j} - x_{C,i})/(2\pi zc)$ and $(i, j) = (\{1, 2\}, \{1', 2'\})$.

Based on the conditions given in Eq.s (26), (27), (28), and in the case considered in Eq.(B.7), we have that

- a For the two double-path labeled by $(1, 1')$ and $(2, 2')$ the Fourier transform reaches approximately its maximum value $FT \{ |A(x_S)|^2 \} (0)$,
- b For the two double-path labeled by $(1, 2')$ and $(1', 2)$ the Fourier transform is approximately zero.

Equation (E.5) can thus be written as

$$\begin{aligned} & G^{(1)}(x_C, \theta_C; x_T, \theta_T) \\ & \simeq C_0 FT \{ |A(x_S)|^2 \} (0) \\ & \times [\cos \theta_C \cos \phi_C \cos(\theta_T - \phi_T) e^{i\omega[x_C^2 - x_T^2]/(2zc)} \\ & + \sin \theta_C \sin \phi_C \sin(\theta_T + \phi_T) e^{i\omega[(x_C + 2\delta_C \bar{z})^2 - (x_T + 2\delta_T \bar{z})^2]/(2zc)}] \\ & = C'_0 [\cos \theta_C \cos \phi_C \cos(\theta_T - \phi_T) \\ & + \sin \theta_C \sin \phi_C \sin(\theta_T + \phi_T) e^{i\phi(x_C, x_T, \delta_C, \delta_T)}], \end{aligned} \quad (\text{E.8})$$

where $C_0 = -(iK'/4) [\omega/(2\pi cz)]^2$ and $C'_0 = C_0 FT \{ |A(x_S)|^2 \} (0)$. By plugging this result in Eq.(C.1), we have

$$\begin{aligned} & \langle \Delta n(x_C, \theta_C) \Delta n(x_T, \theta_T) \rangle \\ & = |C'_0|^2 [\cos \theta_C \cos \phi_C \cos(\theta_T - \phi_T) \\ & + \sin \theta_C \sin \phi_C \sin(\theta_T + \phi_T) e^{i\phi(x_C, x_T, \delta_C, \delta_T)}]^2, \end{aligned} \quad (\text{E.9})$$

which is the result reported in Eq.(29).

Appendix F. Calculation of the propagation matrix $\mathcal{M}'(\kappa)$

In this appendix we calculate the propagation matrix $\mathcal{M}_{d,S}(\kappa)$ introduced in Eq.(E.1).

In the setup of Fig.3 the propagation from the sources (S, S') to the half-wave plates (R_{ϕ_C}, R_{ϕ_T}) is given by the matrix

$$\begin{aligned} \mathcal{U}_{\text{prep}}(\kappa) &:= \mathcal{R} P_1(\kappa) BS_1 P_{ini}(\kappa) \\ &= \frac{1}{\sqrt{2}} \begin{pmatrix} R_{\phi_C} g\{\kappa; S, R_{\phi_C}\} & \imath R_{\phi_C} g\{\kappa; S', R_{\phi_C}\} \\ \imath R_{\phi_T} g\{\kappa; S, R_{\phi_T}\} & R_{\phi_T} g\{\kappa; S', R_{\phi_T}\} \end{pmatrix}, \end{aligned} \quad (\text{F.1})$$

where we have used Eq.s (D.1), (D.2), (D.3), (D.4), (D.5) and (D.11), and $g\{\kappa; s, R_{\phi_i}\}$ is the Green's function propagating the mode κ from the $s = S, S'$ source, to the half-wave plate R_{ϕ_i} with $i = C, T$. The propagation from the half-wave plates R_{ϕ_i} to the points x_C and x_T , defined in the plane of the detector D_C and D_T respectively, is described by the diagonal matrix

$$\mathcal{P}(\kappa) := \text{diag}(\mathcal{P}'_{C,C}(\kappa), \mathcal{P}'_{T,T}(\kappa)), \quad (\text{F.2})$$

with

$$\mathcal{P}'_{C,C}(\kappa) := \imath \text{diag}(g_1\{\kappa; R_{\phi_C}, x_C\}, -g_2\{\kappa; R_{\phi_C}, x_C\}), \quad (\text{F.3})$$

$$\mathcal{P}'_{T,T}(\kappa) := \frac{\imath}{2} (g_{1'}\{\kappa; R_{\phi_T}, x_T\} \mathbb{1} - g_{2'}\{\kappa; R_{\phi_T}, x_T\} F), \quad (\text{F.4})$$

with F defined in Eq.(D.10). By using the results of Eq.s (F.1) and (F.2), we get

$$\begin{aligned} \mathcal{M}'(\kappa) &:= \mathcal{P}(\kappa) \mathcal{U}_{\text{prep}}(\kappa) = \frac{1}{\sqrt{2}} \\ &\times \begin{pmatrix} \mathcal{P}'_{C,C}(\kappa) R_{\phi_C} g\{\kappa; S, R_{\phi_C}\} & \imath \mathcal{P}'_{C,C}(\kappa) R_{\phi_C} g\{\kappa; S', R_{\phi_C}\} \\ \imath \mathcal{P}'_{T,T}(\kappa) R_{\phi_T} g\{\kappa; S, R_{\phi_T}\} & \mathcal{P}'_{T,T}(\kappa) R_{\phi_T} g\{\kappa; S', R_{\phi_T}\} \end{pmatrix} \\ &= \begin{pmatrix} \mathcal{M}'_{C,S}(\kappa) & \mathcal{M}'_{C,S'}(\kappa) \\ \mathcal{M}'_{T,S}(\kappa) & \mathcal{M}'_{T,S'}(\kappa) \end{pmatrix}. \end{aligned} \quad (\text{F.5})$$

- [1] Hanbury Brown R. and Twiss R.Q. 1956 *Nature* **177** 27–29 ISSN 0028-0836 URL <http://dx.doi.org/10.1038/177027a0>
- [2] Hanbury Brown R. and Twiss R.Q. 1956 *Nature* **178** 1046–1048 URL <http://dx.doi.org/10.1038/1781046a0>
- [3] Glauber R.J. 1963 *Phys. Rev. Lett.* **10**(3) 84–86 URL <http://link.aps.org/doi/10.1103/PhysRevLett.10.84>
- [4] Glauber R.J 2005 *Nobel Lecture* **8** URL http://www.nobelprize.org/nobel_prizes/physics/laureates/2005/glauber-lecture.pdf
- [5] Alley C.O. and Shih Y.H. 1986 *Proceedings of the Second International Symposium on Foundations of Quantum Mechanics in the Light of New Technology* ed of Japan P S (Tokyo) pp 47 – 52
Shih Y.H. and Alley C.O. 1988 *Phys. Rev. Lett.* **61**(26) 2921–2924 URL <http://link.aps.org/doi/10.1103/PhysRevLett.61.2921>
- [6] Hong C.K., Ou Z.Y. and Mandel L. 1987 *Phys. Rev. Lett.* **59**(18) 2044–2046 URL <http://link.aps.org/doi/10.1103/PhysRevLett.59.2044>
- [7] Kim H., Kwon O., Kim W., Kim T. 2006 *Phys. Rev. A* **73**, 023820 URL <http://dx.doi.org/10.1103/PhysRevA.73.023820>
- [8] Liu J., Zhou Y., Wang W., Liu R.F., He K., Li F.L., and Xu Z. 2013 *Optics Express* **21**, 16 URL <http://dx.doi.org/10.1364/OE.21.019209>
- [9] Tamma V. and Laibacher S. 2015 *Phys. Rev. Lett.* **114**(24) 243601 URL <http://link.aps.org/doi/10.1103/PhysRevLett.114.243601>
- [10] Tamma V. and Seiler J. 2015, Multipath Correlation Interference with a Thermal Source *arxiv*: 1503.07369 URL <http://arxiv.org/abs/1503.07369>

- [11] Pittman T.B., Shih Y.H., Strekalov D.V. and Sergienko A.V. 1995 *Phys. Rev. A* **52**(5) R3429–R3432 URL <http://link.aps.org/doi/10.1103/PhysRevA.52.R3429>
- [12] Valencia A., Scarcelli G., D’Angelo M. and Shih Y. 2005 *Phys. Rev. Lett.* **94**(6) 063601 URL <http://link.aps.org/doi/10.1103/PhysRevLett.94.063601>
- [13] D’Angelo M., and Shih Y.H. 2005, *Laser Phys. Lett.* **2**, 567 URL <http://dx.doi.org/10.1002/lapl.200510054>
- [14] Scarcelli G., Berardi V. and Shih Y.H. 2006, *Phys. Rev. Lett.* **96**, 063602 URL <http://dx.doi.org/10.1103/PhysRevLett.96.063602>
- [15] Chen H., Peng T. and Shih Y.H. 2013 *Phys. Rev. A* **88**(2) 023808 URL <http://link.aps.org/doi/10.1103/PhysRevA.88.023808>
- [16] Nielsen M. and Chuang I. 2000 *Quantum Computation and Quantum Information* Cambridge Series on Information and the Natural Sciences (Cambridge University Press) ISBN 9780521635035 URL <http://books.google.de/books?id=65FqEKQ0fP8C>
- [17] Tamma V. 2014 *International Journal of Quantum Information* **12** 1560017
- [18] Laibacher S. and Tamma V. 2015 *Phys. Rev. Lett.* **115**(24) 243605 URL <http://link.aps.org/doi/10.1103/PhysRevLett.115.243605>
- [19] Tamma V. and Laibacher S. 2015 *Journal of Modern Optics* 1–5 URL <http://dx.doi.org/10.1080/09500340.2015.1088096>
- [20] Tamma V. and Laibacher S. 2015 *Quantum Inf. Process.* 1–22 ISSN 1570-0755, 1573-1332 URL <http://link.springer.com/10.1007/s11128-015-1177-8>
- [21] D’Angelo M., Chekhova M.V. and Shih Y.H. 2001 *Phys. Rev. Lett.* **87**, 013602 URL <http://dx.doi.org/10.1103/PhysRevLett.87.013602>
- [22] Dowling J., 2008 *Contemporary Physics* **49**, 2 URL <http://dx.doi.org/10.1080/00107510802091298>
- [23] D’Angelo M., Garuccio A. and Tamma V. 2008 *Phys. Rev. A* **77**, 063826 URL <http://dx.doi.org/10.1103/PhysRevA.77.063826>
- [24] Cerf N.J., Adami C. and Kwiat P.G. 1998 *Phys. Rev. A* **57**(3) R1477–R1480 URL <http://link.aps.org/doi/10.1103/PhysRevA.57.R1477>
- [25] Spreuw R.J.C. 2001 *Phys. Rev. A* **63**(6) 062302 URL <http://link.aps.org/doi/10.1103/PhysRevA.63.062302>
- [26] Lee K.F. and Thomas J.E. 2002 *Physical Review Letters* **88** 097902 URL <http://link.aps.org/doi/10.1103/PhysRevLett.88.097902>
- [27] Kagalwala K.H., di Giuseppe G., Abouraddy A.F. and Saleh B.E.A. 2013 *Nature Photonics* **7** 72–78
- [28] Peng T. and Shih Y.H. 2015 *EPL* **112**(6) 60006 URL <http://dx.doi.org/10.1209/0295-5075/112/60006>
- [29] Pittman T.B., Fitch M.J., Jacobs B.C. and Franson J.D. 2003 *Phys. Rev. A* **68**(3) 032316 URL <http://link.aps.org/doi/10.1103/PhysRevA.68.032316>
- [30] O’Brien J.L., Pryde G.J., White A.G., Ralph T.C. and Branning D. 2003 *Nature* **426** 264–267 ISSN 0028-0836 URL <http://dx.doi.org/10.1038/nature02054>
- [31] Sanaka K., Kawahara K. and Kuga T. 2002 *Phys. Rev. A* **66**(4) 040301 URL <http://link.aps.org/doi/10.1103/PhysRevA.66.040301>
- [32] Peng T., Cassano M., Tamma V. and Shih Y.H., to be submitted.
- [33] Glauber R.J. 2007 *Quantum Theory of Optical Coherence: Selected Papers and Lectures* (John Wiley and Sons) ISBN 978-3-527-40687-6
- [34] Mandel L. and Wolf E. 1995 *Optical Coherence and Quantum Optics* (Cambridge University Press) ISBN 9780521417112 URL <http://books.google.de/books?id=FeBix14iM70C>
- [35] Sudarshan E.C.G. 1963 *Phys. Rev. Lett.* **10**(7) 277–279 URL <http://link.aps.org/doi/10.1103/PhysRevLett.10.277>
- [36] Shih Y.H. 2011 *An Introduction to Quantum Optics* (CRC Press Taylor and Francis group)
- [37] Rubin M.H. 1996 *Phys. Rev. A* **54**, 6 URL <http://dx.doi.org/10.1103/PhysRevA.54.5349>